Proceedings of ASME Turbo Expo 2011
GT2011
June 6-10, 2011, Vancouver, British Columbia, Canada

GT2011-46268

EXTENDED MEAN LINE THEORY FOR AXIAL FANS – ANALYTIC CALCULATION OF THE FLOW CHARACTERISTICS FOR OFF-DESIGN POINTS

Matthias Semel
Institute of Fluid Mechanics
University of Erlangen-Nuremberg
Cauerstraße 4
91058 Erlangen
matthias.semel@lstm.uni-erlangen.de

Philipp Epple
Institute of Fluid Mechanics
University of Erlangen-Nuremberg
Cauerstraße 4
91058 Erlangen
philipp.epple@lstm.uni-erlangen.de

Mihai Miclea-Bleiziffer
Institute of Fluid Mechanics
University of Erlangen-Nuremberg
Cauerstraße 4
91058 Erlangen
mihai.miclea@lstm.uni-erlangen.de

Antonio Delgado
Institute of Fluid Mechanics
University of Erlangen-Nuremberg
Cauerstraße 4
91058 Erlangen
antonio.delgado@lstm.uni-erlangen.de

Henrik Smith
Institute of Fluid Mechanics
University of Erlangen-Nuremberg
Cauerstraße 4
91058 Erlangen
henrik.smith@lstm.uni-erlangen.de

ABSTRACT

The use of axial fans is very common for industrial applications. The most common design case is the free vortex design. It ensures constant meridional velocity and hence an axisymmetric and two-dimensional flow. Those designs have proved to be robust and to deliver good results. However, the free vortex model holds only at the design point. At off-design points the flow characteristics differ substantially from the free vortex model, whereby the extent of validity of a forced vortex model is obtained. Solving the equation of radial equilibrium for off-design points enables a more precise design prediction considering the impact of the variable meridional velocity and the angular momentum. This approach can be applied to free vortex models as well as forced vortex models. In the present work theoretical formulas for the flow characteristics at off-design points were developed and implemented. Three angular momentum profiles, one free vortex and two forced vortex models, were analyzed relative to the change in the meridional velocity and angular momentum profiles. The impact of these modifications on the performance characteristics of axial fans, such as pressure, efficiency, torque and hydraulic power was investigated. Comparing design prediction with numerical CFD validation leads to a precise and extensive analysis. The validity of the used approach is demonstrated. Thus a qualitative prediction of flow characteristics for any axial-impeller at off-design is obtained.This allows for a in depth understanding of the fundamental working principles and consequences of the radial equilibrium equation at the design and also at off design points.

INTRODUCTION

Analytic design methods known form the literature, e.g. Eck [1], Eckert and Schnell [2] and Lakshminarayana [3], predict the performance characteristics of the axial impeller only at the design point. Although the change of the mass flow results into a change of the meridional velocity and of the angular momentum distribution, the transfer of such information onto the over and partial load operation regime is actually not considered properly by these theories.

In the classical mean line theory based on the Euler turboma-

chinery equation the flow is solved basically one dimensionally. In this extended theory, the Euler equation is solved taking into account also the radial equilibrium equation. Accordingly to the Euler equation these new equations do not include a loss model. In the present strategy the inviscid equations are solved exactly at design and off-design points in order to obtain the fundamental three dimensional energy transfer and flow pattern in axial fans. The aim of this work is to show the influence of the geometrical parameters of the impeller onto the ideal flow through the machine at any operational point. In order to obtain the real flow pattern in the fan, CFD computations have been performed. Comparing the CFD solutions with the ideal flow solutions it is possible to recognize many fundamental relationships between geometry and flow, which can be used to improve and design impellers. It is not the aim of the ideal flow computations, however, to match the CFD computations quantitatively but qualitatively, showing the relations between geometry and flow patterns, since the ideal flow computations do not include losses. The advantage of this method is, other then using the loss models, which are useful in order to obtain almost exact predictions but do not allow the exact location of the influence of the geometry, is that with this method one can see which geometrical parameter has which influence on the flow, at least qualitatively. Most of the loss models cannot offer this insight. Therefore, this method is an integrated one which requires, in order to obtain also the quantitative characteristics, iteration with CFD computations. The fundamental assumption of negligible radial velocity, i.e. negligible curvature of the stream lines, is confirmed by the CFD results, as will be shown below.

This work includes an analysis and validation of one free vortex and two forced vortex model designs. First geometric parameters and flow characteristics of the three designs will be calculated for the design point. After this the equations for the calculation of variable meridional velocity and the angular momentum will be derived. Finally the total-to-static pressure characteristic for any flow rate, i.e. for the full flow rate characteristic, will be obtained. The new distributions and the resulting performance characteristics will be shown in detail together with a validation with CFD computations.

DESIGN OF DIFFERENT ANGULAR MOMENTUM DISTRIBUTIONS USING THE SIMPLIFIED EQUATION OF RADIAL EQUILIBRIUM

The simplified equation of radial equilibrium is given by Lakshminarayana [3]:

$$\frac{dp_t}{dr} = 2 \cdot \pi \cdot n \frac{d\left(r \cdot c_{u2}\right)}{dr} = \frac{c_{u2}}{r} \frac{d\left(r \cdot c_{u2}\right)}{dr} + c_{m2} \frac{dc_{m2}}{dr} \qquad (1)$$

With n being the number of revolutions per time unit, $r \cdot c_{u2}$ is the angular momentum and c_{m2} is the meridional velocity of the fluid at the exit of the blade. In the simplified equation for radial equilibrium it is assumed that the radial component of the velocity is negligible before the flow enters and after the flow exits the blade (Carolus [4]). Rearranging the terms and interpreting the velocity c_u as the angular velocity of the fluid relative to the rotational axis of the impeller at a specific radius times the radius $\omega_f = \frac{c_u}{r}$ the following equation

$$\left(\omega_{imp} - \omega_f\right) \cdot \frac{d\left(r^2 \cdot \omega_f\right)}{dr} = c_{m2} \frac{dc_{m2}}{dr} \qquad (2)$$

is obtained. ω_{imp} is the angular velocity of the impeller. This approach has proven to be useful in treating the simplified equation of radial equilibrium mathematically. Of course the angular velocity of the fluid is related to the angular velocity of the impeller through the local head coefficient, i.e.

$$\psi(r) = \frac{\omega_f}{\omega_{imp}} \qquad (3)$$

so that one can compute the head coefficient directly form the angular velocity of the fluid, they are perfectly equivalent.
Equation (2) is a first order ordinary differential equation and can be solved either for any given angular momentum distribution $\omega_f \cdot r^2$ or for any meridional velocity distribution. If the angular momentum is chosen the solution is the corresponding meridional velocity. In the literature, e.g. Carolus [4], two different concepts of designs are defined. The design is named free vortex design, if the angular momentum is chosen as being constant over the radius. In the case where the angular momentum is chosen as being a function depending on the radius, the design is called forced vortex design. Hence, there is only one possible free vortex design but a wide variety of forced vortex designs. The free vortex design is the most widely accepted and used design case (Lakshminarayana [3], Carolus [4]).

Free Vortex Design – Constant Angular Momentum

The well known model of the free vortex design corresponds to a constant angular momentum distribution $f(r)$ at the design point as shown in figure 1.

The prescribed angular momentum distribution is constant over the radius (f const.). The maximal possible angular momentum determined by the rotational velocity of the impeller is increasing parabolically ($\omega_{impeller} \cdot r^2$). The angular velocity of the fluid ω_f is decreasing with $\frac{1}{r^2}$ from the hub to the shroud, while the angular velocity of the impeller ω_{imp} is constant.

$$f(r) = r^2 \cdot \omega_{f,k} = const. = K \qquad (4)$$

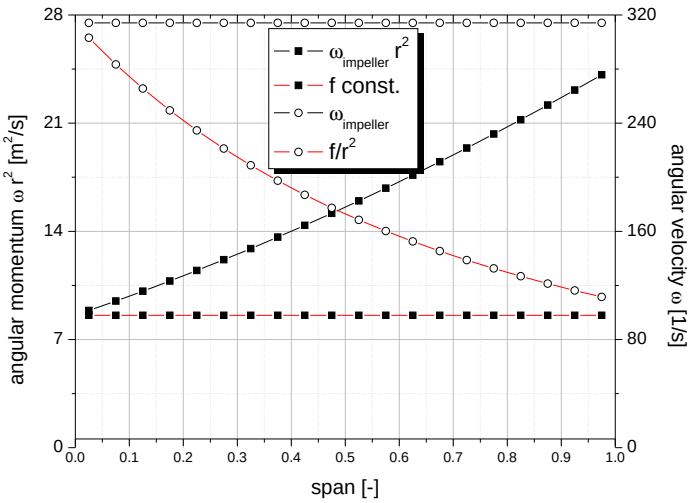

FIGURE 1. CONSTANT ANGULAR MOMENTUM
ANGULAR MOMENTUM AND VELOCITY DISTRIBUTION

K is a constant angular momentum. Insertion eq. (4) into the SRE equation (2) leads to:

$$\begin{aligned} c_{m2}\frac{dc_{m2}}{dr} &= \left(\omega_{imp}-\omega_f\right)\frac{dK}{dr} \\ c_{m2}\frac{dc_{m2}}{dr} &= 0 \end{aligned} \tag{5}$$

And finally the flow parameters are determined as:

$$\begin{aligned} c_{m2} &= \frac{Q}{r_{ti}^2\cdot\left(1-m^2\right)\cdot\pi} = const. \\ \omega_f &= \frac{K}{r^2} \end{aligned} \tag{6}$$

Where m is the hub to tip ratio and r_{ti} is the radius at the blade tip. Hence the meridional velocity is constant over the radius at the area behind the blade. However, it has to be mentioned, that this result is valid only at the design point. For all other flow conditions it will change with the radius.

For the free vortex model there is a gap between the maximal usable angular momentum ($\omega_{imp}\cdot r^2$) and the actually used angular momentum ($f(r)=const.$) as shown in figure 1. Closer to the shroud the distance between those two distributions gets larger. The work of such an impeller is determined by $r_{shroud}^2\cdot\omega_{imp}$. Considering an axial impeller as a machine using just the change in the angular momentum, designs operating with a wider range of the maximal usable angular momentum seem to be promising.

Forced Vortex Design – Constant Angular Velocity

A first approach could be a similar distribution (fig.2: ω_c) as the angular momentum distribution of the impeller (fig.2: ω_{imp}).

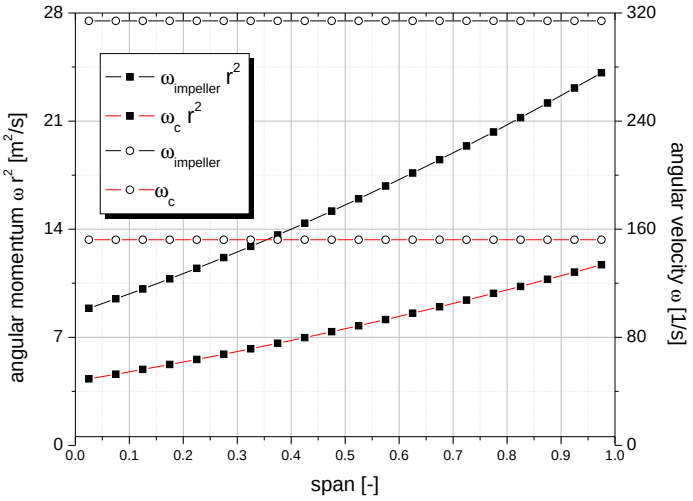

FIGURE 2. CONSTANT ANGULAR VELOCITY
ANGULAR MOMENTUM AND VELOCITY DISTRIBUTION

This results in an angular momentum as shown in figure 2 ($\omega_{imp}\cdot r^2$,$\omega_{f,c}\cdot r^2$).

$$\begin{aligned} f(r) &= c_u\cdot r = \omega_f(r)\cdot r^2 \\ \omega_f(r) &= \omega_{f,c} = const. \end{aligned} \tag{7}$$

Inserting this model into the SRE equation (2):

$$\begin{aligned} r^2\cdot\omega_{f,c}\cdot\left(\omega_{imp}-\omega_{f,c}\right)+C &= \frac{1}{2}c_{m2}^2 \\ c_{m2} &= \sqrt{2r^2\cdot\omega_{f,c}\cdot\left(\omega_{imp}-\omega_{f,c}\right)+C} \\ c_{m2} &= r\cdot\omega_{imp}\sqrt{2\underbrace{\psi_c\cdot\left(1-\psi_c\right)}_{A}+\frac{C}{r^2}} \end{aligned} \tag{8}$$

Here the definition of the local head coefficient ψ and the local flow coefficient φ was used according to Lewis [5]:

$$\psi=\frac{\omega_f}{\omega_{imp}} \qquad \varphi=\frac{c_m}{\omega_{imp}\cdot r} \tag{9}$$

Applying the continuity equation in the integral form the con-

stant C can be defined:

$$Q = \int_{m \cdot r_{ti}}^{r_{ti}} 2\pi \cdot r \cdot c_{m2}(r) dr \tag{10}$$

In contrast to the free vortex design, where the working volume flow can be chosen arbitrarily, there is a flow rate constrain for this kind of forced vortex design. The smallest possible flow rate is than determined by the constant C in such a way that the term under the root is greater zero.

$$\begin{aligned} C &\geq -2 \cdot r^2 \cdot A \\ C &\geq -2 \cdot A \cdot m^2 \cdot r_{ti}^2 \end{aligned} \tag{11}$$

The minimal working flow rate is determined by:

$$Q_{min} = \frac{2}{3}\sqrt{2 \cdot A \cdot (1-m^2)} \cdot \omega_{imp} \cdot \sqrt{2} \cdot r_{ti}^3 \cdot \left(1-m^2\right) \tag{12}$$

Forced Vortex Design – Linear Angular Velocity

In order to get a better understanding for forced vortex designs the angular velocity profile was chosen to be linear with a negative slope as shown in figure 3 (ω_l). The corresponding angular momentum distribution can be seen in figure 3 ($\omega_l \cdot r^2$).

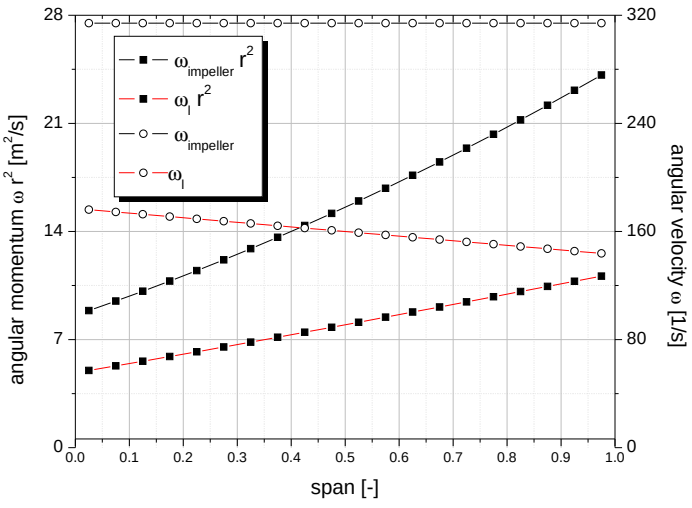

FIGURE 3. LINEAR ANGULAR VELOCITY
ANGULAR MOMENTUM AND VELOCITY DISTRIBUTION

The angular velocity of the fluid is defined as follows:

$$\begin{aligned} \omega_f(r) &= \omega_{impeller} \cdot \left(a - b \cdot \frac{1-\frac{r}{r_{ti}}}{1-m}\right) \\ a \in [0,1], \;\; b &\in [-1,1], \;\; \forall a,b \;\; 0 \leq \frac{\omega_f(r)}{\omega_{imp}} \leq 1 \end{aligned} \tag{13}$$

Here a is giving the starting level of the angular velocity at the shroud, while b represents the difference in the angular velocity from shroud to hub. Therefore, $a = \omega_{f,c}$ and $b = 0$ is equivalent to the constant angular velocity $\omega_{f,c}$. The SRE equation (2) results in

$$c_{m,2} = \frac{\omega_{imp} \cdot r}{6 r_{ti} \cdot (1-m)} \sqrt{a_1 \cdot r^2 + a_2 \cdot r + a_3 + \frac{C}{r^2}} \tag{14}$$

with

$$\begin{aligned} a_1 &= -54 \cdot b^2 \\ a_2 &= b \cdot r_{ti} \cdot [72 \cdot (1-m) + 120 \cdot (b - a \cdot (1-m))] \\ a_3 &= 72 \cdot r_{ti}^2 \cdot [a \cdot (1-m)^2 - b \cdot (1-m) - (a-b)^2 \\ &\quad + 2 \cdot a^2 \cdot m \cdot (1-m) - 2a \cdot m \cdot b] \\ C_{min} &\geq m^2 \cdot r_{ti}^2 \left[-a_1 \cdot m^2 \cdot r_{ti}^2 - a_2 \cdot m \cdot r_{ti} - a_3\right] \end{aligned} \tag{15}$$

Comparision Of The Three Design Cases

For comparison of this three design models, the configuration in table 1 was used.

Δp_t	:	3185 [Pa]
m	:	$\frac{59}{100}$
Q	:	6.4 [m^3/s]
r_{ti}	:	0.28 [m]
n	:	3000 [1/min]

TABLE 1. DESIGN PARAMETER

The three different designs result in three flow angle distributions as shown in fig.4.

The free vortex design (fig.4: f constant) has a high angle at the hub declining nearer to the shroud. The angle of the constant angular velocity (fig.4: ω_c) is small at the hub and increasing to the shroud. The linear angular velocity (fig.4: ω_l) results in a rather constant angle distribution. The free vortex design is nearly working at its maximum according to the angular momentum level at this design point. β_2 values higher than 90° are

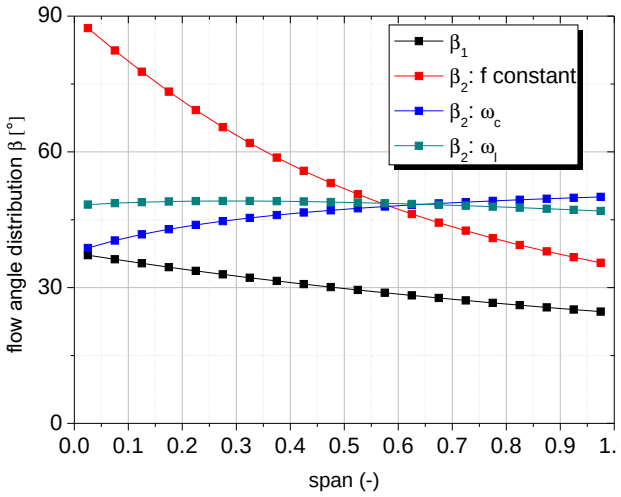

FIGURE 4. FLOW ANGLE DISTRIBUTION

not reasonable. On the contrary the forced vortex designs are working on a rather low level. It is difficult to find operating conditions in which the forced vortex designs as well as the free vortex design work. Either the entry angle β_1 is higher than the exit angle for the forced vortex designs or the exit angle of the free vortex design exceed 90°. The flow turning angle, i.e. the change in the angle between blade inlet and outlet $\beta_2 r - \beta_1 r$, is shown in figure 5.

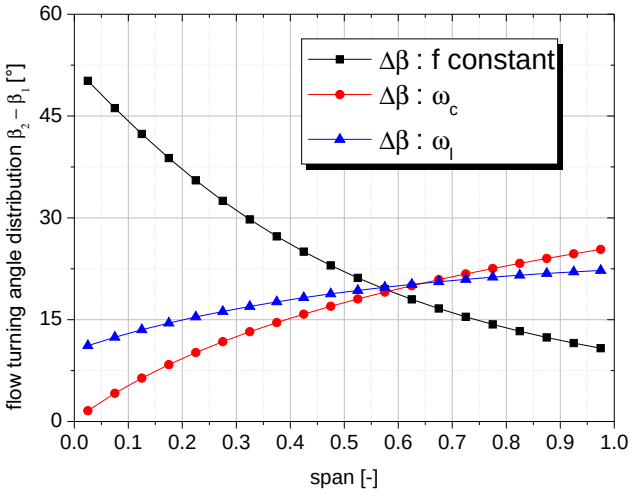

FIGURE 5. FLOW TURNING ANGLE DISTRIBUTION

Both forced vortex designs are demanding small and slightly increasing flow turning angles, while the free vortex design requires a high flow turning angle at the hub and a decreasing flow turning angle toward the shroud. The uniformly distributed work of the free vortex design is connected with a high flow turning angle, which implies the danger of a flow separation at too high flow turning angle and rather complicated blade geometries. Both forced vortex designs are not so demanding concerning the flow turning angle, being less prone to flow separation and resulting in smoother blade geometries.

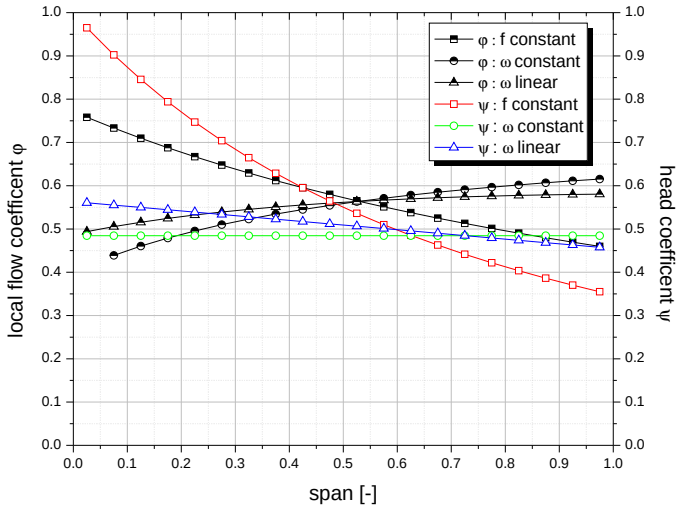

FIGURE 6. HEAD AND FLOW COEFFICENT DISTRIBUTION

The local head and flow coefficient distributions of the three designs are shown in fig.6. For the linear angular velocity the head coefficient is linearly decreasing from hub to shroud (ψ: ω linear). The head coefficient of the constant angular velocity is constant (ψ: ω constant), while the constant angular momentum distribution is decreasing with $\frac{1}{r^2}$(ψ: f constanrt). Considering the definition of the head coefficient as

$$\psi = \frac{\Delta p_t}{\rho \cdot r^2 \cdot \omega_{impeller}} = \frac{u \cdot c_u}{u^2} = \frac{\omega_f}{\omega_{imp}} \tag{16}$$

this distribution is easier to understand. Prescribing the angular velocity of the fluid is equivalent to prescribing the total pressure distribution over the blade. The flow coefficient for both forced vortex designs is increasing from hub to shroud, while the free vortex design is decreasing. The blade angle distribution is now defined and a blade can be computed. In order to get the pressure performance characteristics of this impeller a calculating method for the off-design condition has to be developed. First the method to calculate the change in the meridional velocity profile and in the angular momentum distribution due to a change in the volume flow will be derived and after this a method to calculate the actual pressure distribution.

CALCULATION METHOD TO DETERMINATE THE ACTUAL MERDIONAL VELOCITY DISTRIBUTION AT ANY FLOWRATE

For any flow rate the radial equilibrium equation has to be fulfilled

$$\left(\omega_{imp}-\omega_{f2}\right)\cdot\frac{dr^2\omega_{f2}}{dr}=c_{m2}\frac{dc_{m2}}{dr} \tag{17}$$

$$\frac{1}{r\cdot\tan\beta_{2,0}}\cdot\frac{dr^2\omega_{f2}}{dr}=c_{m2}\frac{dc_{m2}}{dr} \tag{18}$$

Having designed a blade at a specific design point the distribution of β_2 is fixed.

$$c_{u2}=\frac{f(r)}{r}=r\cdot\omega_{imp}-\frac{c_{m2}}{\tan\beta_2} \tag{19}$$

Or rearranged

$$\frac{1}{\tan\beta_2}=\frac{r\cdot\left(\omega_{imp}-\omega_{f,0}\right)}{c_{m2,0}} \tag{20}$$

For an ideal axial fan this angle distribution relates the constant angular velocity of the impeller $\omega_{impeller}$ and the actual meridional velocity c_{m2} to the actual angular velocity of the fluid ω_f.

$$\frac{1}{\tan\beta_2}=\frac{r\cdot\left(\omega_{imp}-\omega_{f}\right)}{c_{m2}} \tag{21}$$

Substituting equation (20) in the equation of radial equilibrium (2) a connection between the design point and the actual working point of the impeller is achieved.

$$\frac{dr^2\omega_{f2}}{dr}=\frac{c_{m2,0}}{\left(\omega_{imp}-\omega_{f,0}\right)}\frac{dc_{m2}}{dr} \tag{22}$$

The derivation of the angular momentum is

$$\begin{aligned}\frac{dr^2\omega_f}{dr}&=-\frac{r^2}{c_{m,0}}\cdot\left(\omega_{imp}-\omega_{f,0}\right)\cdot\frac{c_m}{dr}+2\cdot r\cdot\omega_{imp}\\&=\left[\frac{r^2}{c_{m,0}^2}\cdot\left(\left[\frac{dc_{m,0}}{dr}-\frac{2c_{m,0}}{r}\right]\cdot\left(\omega_{imp}-\omega_{f,0}\right)\right)\right]\cdot c_m\end{aligned} \tag{23}$$

Substituting this into the equation of radial equilibrium, rearranging the terms, and using the definitions of the head coefficient and the flow coefficient, eq. (9), the following equation can be derived:

$$\frac{dc_m}{dr}+p(r)\cdot c_m=s(r) \tag{24}$$

with

$$\begin{aligned}p(r)&=-\tfrac{1}{\varphi\cdot r\cdot\omega_{imp}}\cdot\tfrac{dc_{m,0}}{dr}+\underbrace{\frac{2\cdot(1-\psi)}{r\cdot\left(\varphi^2+(1-\psi)^2\right)}}_{p_2}\\s(r)&=2\tfrac{\omega_{imp}\cdot(1-\psi)\cdot\varphi}{\left(\varphi^2+(1-\psi)^2\right)}\end{aligned} \tag{25}$$

This is a first order ordinary differential equation and its general solution is given by Boyce and DiPrima [6] defined as:

$$c_m=e^{-\int p(r)dr}\cdot\left[s(r)\cdot e^{\int p(r)dr}\int dr+C\right] \tag{26}$$

This constant should be determined by the actual flow rate constraint:

$$Q=2\pi\cdot\int_{m\cdot r_{ti}}^{r_{ti}}r\cdot c_m dr \tag{27}$$

After some algebra the general solution for this equation is derived:

$$\begin{aligned}c_{m,2}(r,p)&=c_{m,2}(r)\cdot\left[1+C(p)\cdot e^{-\int p_2(r)dr}\right]\\C(p)&=\tfrac{Q_0\cdot(p-1)}{2\cdot\pi\int r\cdot e^{-\int p_2 dr}dr}\end{aligned} \tag{28}$$

p is the ration between the actual flow rate Q and the design flow rate Q_0.

$$p=\frac{Q}{Q_0} \tag{29}$$

With this method it is possible to compute a theoretically more accurate head - flow characteristic of an axial impeller considering also the change in the angular momentum and the meridional velocity. Using this method enables an analytical comparison between forced vortex and free vortex designs.

CALCULATION OF THE TOTAL-TO-STATIC PRESSURE INCREASE FOR ANY OPERATION POINT

According to the extended mean line design theory (Epple [7], [8], [9]), the static pressure rise at a specific radius section of an axial fan is given by

$$\Delta p_{s,section} = \frac{\rho}{2} \cdot \left(w_1^2 - w_2^2\right) \tag{30}$$

The total-to-static pressure rise is given by

$$\Delta p_{t-s,section} = \Delta p_s - \frac{\rho}{2} c_1^2 \tag{31}$$

Considering the no pre-swirl flow entry

$$w_1^2 = u^2 + c_1^2 \tag{32}$$

and substituting this equation into (31) leads to

$$\Delta p_{t-s,section} = \frac{\rho}{2}\left(u^2 - w_2^2\right) = \frac{\rho}{2}\left[u^2 - \left(\frac{c_{m2}}{\sin\beta_2}\right)^2\right] \tag{33}$$

$$\Delta p_{t-s,section} = \frac{\rho}{2}\left[u^2 - \left(1 + \frac{1}{\tan^2\beta_2}\right) \cdot c_{m2}^2\right] \tag{34}$$

Combining (34) with (21) the total-to-static pressure rise can be given for any flowrate

$$\begin{aligned} \Delta p_{t-s,section} &= \frac{\rho}{2} \cdot \left[r^2 \cdot \omega_{imp} - c_m^2 - r^2 \cdot \left(\omega_{imp} - \omega_f\right)^2\right] \\ \Delta p_{t-s,section} &= \frac{\rho}{2} \cdot \left[2r^2 \cdot \omega_f \cdot \omega_{imp} - c_m^2 - r^2\omega_f^2\right] \\ \Delta p_{t-s,section} &= \frac{\rho}{2} \cdot \left[2 \cdot \frac{1}{\rho}\Delta p_{t,section} - c_m^2 - c_u^2\right] \end{aligned} \tag{35}$$

In order to get the pressure rise of the whole axial fan the mass flow average over the complete impeller surface has to be taken:

$$\Delta p_{t-s} = \frac{1}{\rho \cdot Q} \int_{m \cdot r_{ti}}^{r_{ti}} 2\pi \cdot \rho \cdot r \cdot \Delta p_{t-s,section}(r,p) \cdot c_{m2}(r,p) dr \tag{36}$$

$$\Delta p_{t-s}(p) = \frac{\pi \cdot \rho}{Q} \int_{m \cdot r_{ti}}^{r_{ti}} r \cdot c_{m2}\left(2\Delta p_{t,section} - c_{m2}^2 - c_u^2\right) dr \tag{37}$$

With this equation it is possible to calculate the actual pressure rise of the fan for any flow rate. Therefore the actual meridional velocity and the actual angular momentum distribution - or total pressure distribution - is required.

CASE STUDY – ANALYTICAL SOLUTION FOR THE THREE DIFFERENT MERIDIONAL VELOCITY PROFILES AND COMPARISION WITH CFD RESULTS

The meridional velocity distribution, the angular momentum distribution and the pressure distribution were computed with the presented method for the three designs cases. For the validation of the method CFD computations were performed. The computation was done for an impeller with 17 blades. The blade shape was derived by inverse calculation of a NACA 4 digit airfoil camber line. First the method for inversely calculating the camber line will be presented and after this the configuration of the simulation will be shown.

Inverse Camber Line Calculation

The three parameters necessary for the complete definition of such a camber line are the maximum camber f, the position of maximum camber g and the thickness t. The CFD simulation should illustrate the flow behavior without to many disturbing parameters, so the thickness t was kept constant at a value of $t = 0.025 \cdot l$. While the last parameter can be given independently, the first two have to be calculated inversely depending on the desired inlet and outlet blade angles. According to Lakshminarayana [3] the blade turning angle is defined as

$$\Delta\beta = \beta_2 - \beta_1 \quad . \tag{38}$$

It is segmented into γ_1 and γ_2 (see fig. 7) by means of a balancing factor *bal* that has to be chosen in the range $0 < bal < 1$:

$$\gamma_1 = bal \cdot \Delta\beta \tag{39}$$

$$\gamma_2 = (1 - bal) \cdot \Delta\beta \quad . \tag{40}$$

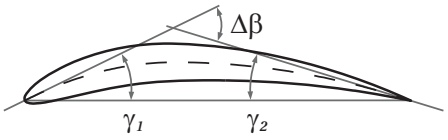

FIGURE 7. PARAMETERS FOR THE INVERSE DEFINITION OF A NACA 4 DIGIT PROFILE

This is sufficient to get f and g using a set of two linear equations. The camber lines were generated with a balancing factor of $bal = 0.3$. With bal set, γ_1 and consequently the stagger angle can be calculated as:

$$\lambda = \beta_{1,p} - \gamma_1 \quad . \tag{41}$$

CFD-Simulation Configuration

The 3D CFD simulations are performed with ANSYS CFX®12.1. To reduce complexity, the hub and shroud radii are kept constant from inlet to outlet and a tip gap is not modeled. The 3D CFD simulations are performed modeling a single passage using a rotational periodicity interface and a constant pitch of $21,17^\circ$ according to the blade number of $z = 17$.

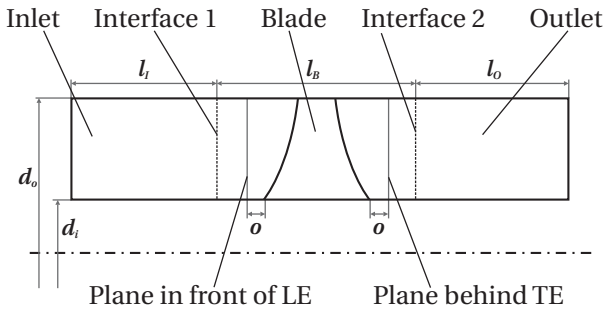

FIGURE 8. SIMULATION SETUP

The simulation is composed of three domains – inlet, blade and outlet (see fig. 8). Missing basic dimensions can be found in tab. 2. They are connected by means of a *Frozen Rotor* interface. The grid consists of 100000 hexa-elements. The inlet and outlet region used the same mesh with 30000 Elements. For the blade channel 40000 Elements were used. A block-structured hexahedral grid is used for all three domains including an O-Grid around the blade. The mesh density is increased in the near-wall regions of the blade,hub and shroud. A grid study was performed to ensure the independence of the solution from the number of nodes.

The boundary condition at the walls is *free-slip* and the inlet boundary condition is set to a mass flow according to the flow rate and a reference density of $\rho_a = 1.184\,\mathrm{kg/m^3}$. A reference pressure of $p_a = 101325$ Pa is set at the outlet and a static temperature of $T_a = 25\,^\circ$C. All CFD simulations were performed using the *Shear Stress Transport* turbulence model e.g. Menter [10].

Parameter	Variable	Value
Inlet axial length	l_I	1.4 m
Blade axial length	l_B	0.1 m
Outlet axial length	l_O	1.4 m
Axial offset	o	0.03 m

TABLE 2. BASIC DIMENSIONS OF THE SIMULATION SETUP

Radial Velocity

The derived equations are valid for the condition of negligible radial velocities in the plane before entering and after exiting the impeller. To verify this condition the radial velocity distribution was investigated at the planes "Plane in front of LE" and "Plane behind TE" (fig.8) for different flow rates. Figure 9 points the ratio of the radial velocity to the meridional velocity c_r/c_m at different flow rates. The ratio is very low behind the blade for every design case and at every flow rate. In front of the blade the ratio is slightly higher, but it is still on a low level. This result demonstrates that the assumption of negligible radial velocities holds very well. So the constrains for the derived equations are fulfilled.

Free Vortex Design - Constant Angular Momentum

Figure 10 depicts the change in the angular momentum distribution due to different flow rates. For the design case the angular momentum is constant (fig.10 Q=6.4 $[\mathrm{m^3/s}]$ design). At the overload regime the angular momentum changes to a lower level (fig.10 Q=7.5 $[\mathrm{m^3/s}]$ design & Q=8.0 $[\mathrm{m^3/s}]$ design). In the overload regime the angular momentum drops slightly form hub to shroud. The drop of the angular momentum from hub to shroud is higher the higher the flow rate. For partial load the whole behavior is reversed at the design point distribution. I.e. the higher the flow rate the higher the angular momentum (fig.10 Q=5.0 $[\mathrm{m^3/s}]$ design & Q=5.5 $[\mathrm{m^3/s}]$ design). It is worth mentioning that the design angular momentum distributions are symmetric with reference to the horizontal angular momentum characteristic at the design point.

All the angular momentum distributions of the CFD simulation possess qualitatively the same shape: High values at the hub reducing toward the shroud (fig.10 Q=5.0 $[\mathrm{m^3/s}]$ CFD - Q=8.0 $[\mathrm{m^3/s}]$ CFD). The difference of the angular momentum between hub and shroud gets more pronounced at higher flow rates. At none of these distributions the design goal of a constant angular momentum distribution was achieved. This prescribed condition is shifted to a flow rate below Q=5.0 $[\mathrm{m^3/s}]$. Moreover the constant angular momentum level of the CFD-simulation will be on a lower level than the design level.

One has to keep in mind, that it is not the aim to fully model

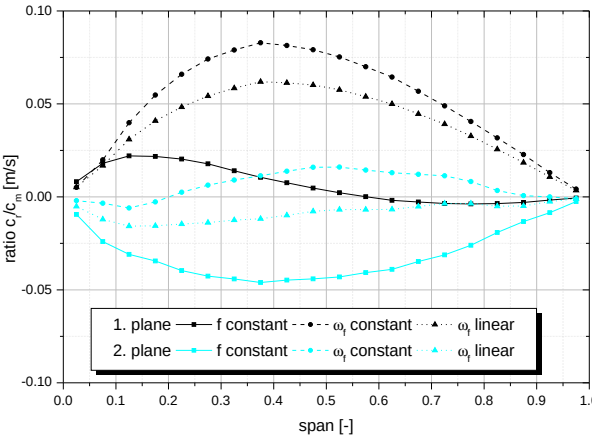

(a) Q = 5.0 m^3/s

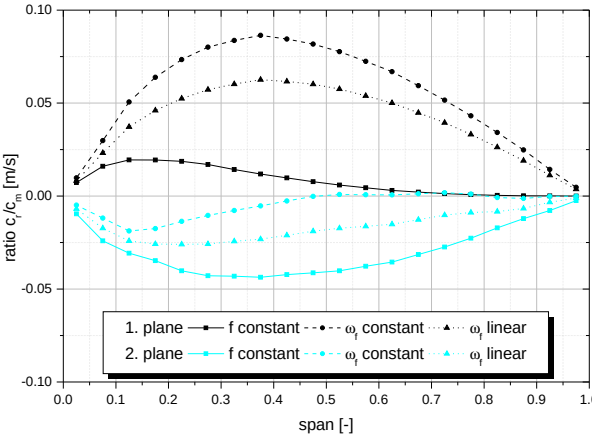

(b) Q = 6.4 m^3/s

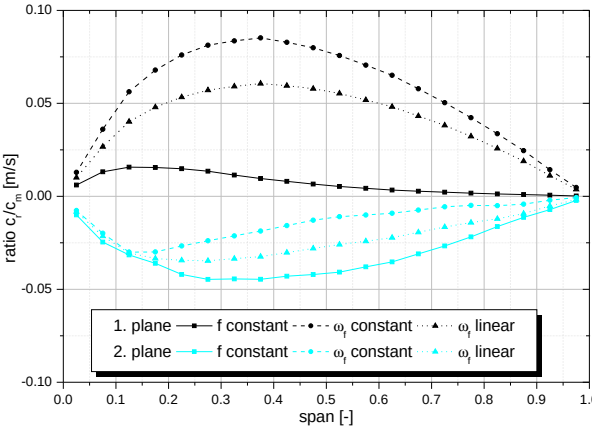

(c) Q = 8.0 m^3/s

FIGURE 9. RATIO c_r/c_m AT DIFFERENT FLOW RATES

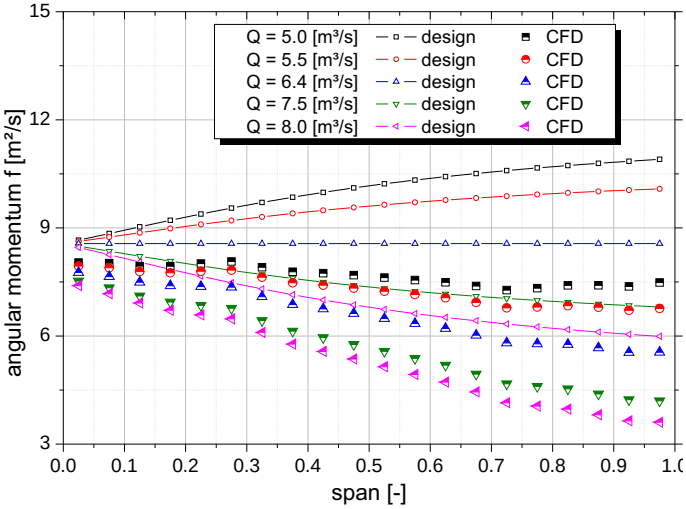

FIGURE 10. CONSTANT ANGULAR MOMENTUM ANGULAR MOMENTUM DISTRIBUTION

the real characteristics e.g. with loss models in order to match the CFD solutions, but to show the fundamental dependencies in a qualitative way. The one dimensional method is predicting the flow characteristics for an ideal flow. The CFD-calculations are showing the real flow behavior. Consequently the influence of the blade geometry, influence of the blade number, viscid losses and the difference between flow angle and blade angle are included. An optimal blade geometry forces the real flow to always follow the blade angle. In this way nearly a ideal flow solution can be obtained. In this validation a not optimized blade geometry was used, so a difference between flow angle and blade angle is likely to occur. This will result in differences between CFD prediction and design prediction. But as the real flow is connected to the ideal flow solution, this method should show a qualitative conformity.

As explained above, the results of the CFD calculations, i.e. Q *in* [5-8] m^3/s (fig. 10) have to be interpreted as the flow behavior at *overload regime*. Comparing the design curves with the corresponding CFD curves it is visible that all CFD curves behave qualitatively like the design curves at over load. That means that when going from design to CFD there is a shift of the angular momentum characteristics toward over load. Consequently the curves in fig.10 Q=5.0 $[m^3/s]$ CFD - Q=8.0 $[m^3/s]$ CFD have to qualitatively match with the design distributions at overload (Q=7.5 $[m^3/s]$ design & Q=8.0 $[m^3/s]$ design). All the CFD-distributions comply with this requirement. They all have qualitatively the same shape as the design distributions at overload, but the whole level is shifted a bit to a lower angular momentum.

Figure 11 shows the change in the meridional velocity due to different flow rates. For the design case the meridional velocity

is constant (fig.11 Q=6.4 [m^3/s] design). If the impeller is working at a higher flow rate as the design point, it will be working in *overload* and hence, the meridional velocity will change from a constant meridional velocity to a variable velocity with lower velocities at the hub and higher velocities at the shroud (fig.11 Q=7.5 [m^3/s] design & Q=8.0 [m^3/s] design). For increasing flow rates this behavior becomes more pronounced. For an impeller working in *partial load* the whole behavior is reversed. Then, higher velocities can be found at the shroud and lower velocities at the hub (fig.11 Q=5.0 [m^3/s] design & Q=5.5 [m^3/s] design).

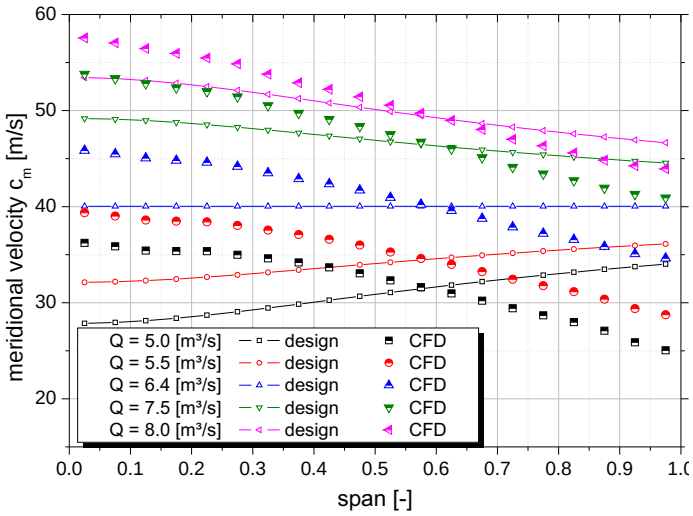

FIGURE 11. CONSTANT ANGULAR MOMENTUM MERIDIONAL VELOCITY DISTRIBUTION

All the meridional velocity distributions of the CFD simulation possess qualitatively the same shape: High values at the hub reducing toward the shroud (fig.11 Q=5.0 [m^3/s] CFD - Q=8.0 [m^3/s] CFD). The difference of the meridional velocity between hub and shroud gets more pronounced at higher flow rates. This result is also expected, since the ideal machine reaches higher flow rates than the real machine or CFD computations, since losses do not occur. The losses and the non blade congruent flow in the real machine cause a drop in the maximum flow rate and hence the real machine operates at higher flow rates, as compared to the ideal machine. The analysis of the angular momentum distribution has demonstrated, that the CFD-distributions have to be interpreted as distributions in *overload regime*. Consequently the curves in fig.11 Q=5.0 [m^3/s] CFD - Q=8.0 [m^3/s] CFD have to qualitatively match with the design distributions at overload (Q=7.5 [m^3/s] design & Q=8.0 [m^3/s] design). All the CFD-distributions comply with this requirement. They all have qualitatively the same shape as the design distributions at overload. The comparison of both distributions, meridional velocity and angular momentum, indicate a good qualitative consistence between the design prediction and the CFD-simulations.

Forced Vortex Design – Constant Angular Velocity

Figure 12 shows the change in the angular velocity due to different flow rates. For the design case the angular velocity is constant (fig.12 Q=6.4 [m^3/s] design). At overload the angular velocity drops to a lower level with low values at the hub increasing to the shroud in a way similar to the negative root-function with a low slope (fig.12 Q=7.5 [m^3/s] design & Q=8.0 [m^3/s] design). Like the free vortex design the whole behavior is mirrored around the design point distribution. The angular velocity is rising from hub to shroud (fig.12 Q=5.0 [m^3/s] design & Q=5.5 [m^3/s] design).

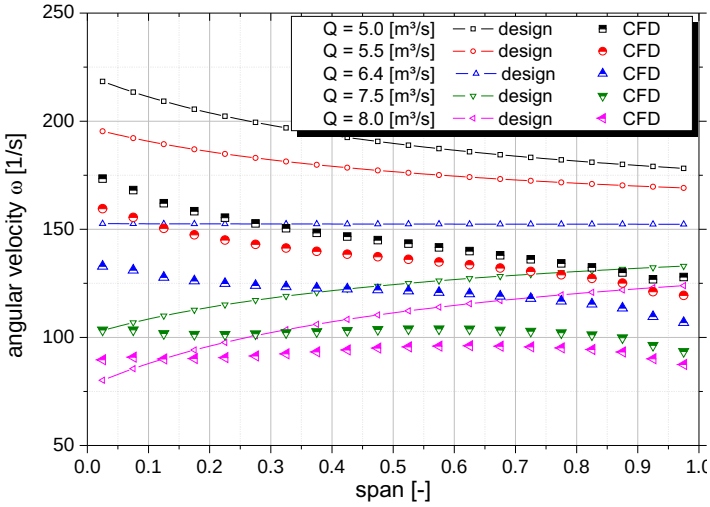

FIGURE 12. CONSTANT ANGULAR VELOCITY ANGULAR VELOCITY DISTRIBUTION

The angular velocity distributions of the CFD simulations are also depicted in figure 12. The distributions at low and moderate flow rates (Q=5.0 [m^3/s] - Q=6.4 [m^3/s] CFD) show high velocities at the hub decreasing to the shroud in a shape similar to a negative root-function. This behavior gets less pronounced at higher flow rates. At the flow rate Q=7.5 [m^3/s] CFD a nearly constant angular velocity distribution is reached. Low values at the hub increasing to the shroud in the shape of a very flat positive root function can be seen at flow rate Q=8.0 [m^3/s] CFD.

The CFD simulation reaches the design goal of constant angular velocity at a flow rate of Q=7.5 [m^3/s] CFD. The impeller is working in *overload* at a flow rate of Q=8.0 [m^3/s] CFD. For the flow rates Q=5.0 [m^3/s] CFD - Q=6.4 [m^3/s]

CFD the impeller is at *partial load*. The distributions of Q=5.0 [m^3/s] CFD - Q=6.4 [m^3/s] CFD qualitatively match the curves of Q=5.0 [m^3/s] design & Q=5.5 [m^3/s] design. Also the curve at *overload* Q=8.0 [m^3/s] CFD show similar behavior to Q=7.5 [m^3/s] design & Q=8.0 [m^3/s] design. This probe shows a good conformity between design prediction and CFD-simulation. The partial load as well as the overload prediction is qualitatively matched by the CFD-simulation.

Figure 13 shows the change in the meridional velocity due to different flow rates. For the design case the meridional velocity is an almost linear curve with a positive slope (fig.13 Q=6.4 [m^3/s] design). In overload the meridional velocity distribution is pushed to a higher level with the same slope and same shape (fig.13 Q=7.5 [m^3/s] design & 13 Q=8.0 [m^3/s] design). In partial load the meridional velocity distribution is pushed to a lower level with the same slope and the same shape (fig.13 Q=5.0 [m^3/s] design & 13 Q=5.5 [m^3/s] design).

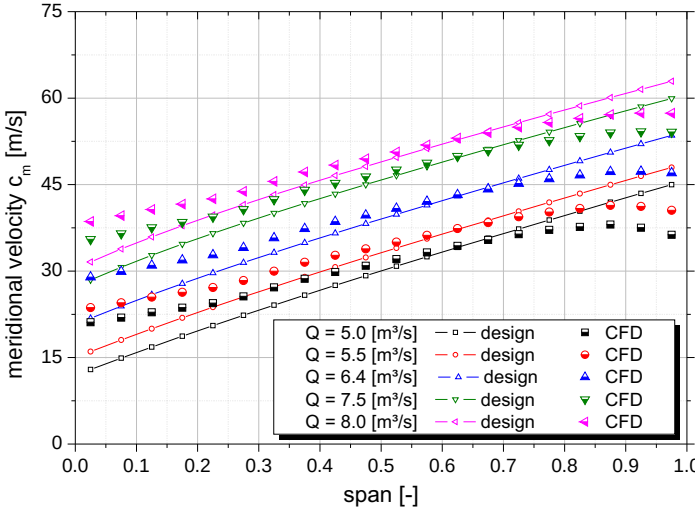

FIGURE 13. CONSTANT ANGULAR VELOCITY MERIDIONAL VELOCITY DISTRIBUTION

The results of the CFD-simulations show also a linear meridional velocity distribution (fig.13 Q=5.0 [m^3/s] CFD - 13 Q=8.0 [m^3/s] CFD). But the slope of these distribution is lower compared to the slope of the design prediction. The angular velocity examination has shown, that the prescribed angular velocity distribution is achieved at a higher flow rate at a lower level. This difference results into a different slope for the meridional velocity (compare eq. (8)). The prediction of a parallel shift of the meridional velocity distribution with the same slope of the design method is qualitatively fulfilled. In such a way a qualitatively consistence between the design prediction and the CFD-simulations for the forced vortex design of constant angular velocity is achieved.

Forced Vortex Design – Linear Angular Velocity Of The Fluid

Figure 14 shows the change in the angular velocity due to different flow rates. For the design case the angular velocity is a straight line with negative slope (fig.14 Q=6.4 [m^3/s] design). The distributions of the design prediction are similar to the distribution of the constant angular velocity prediction. Here all distributions are tilted rightwards. At overload the angular velocity drops to a lower level with low values at the shroud increasing to the hub in a shape similar to the superposition of a straight linear with negative slope and a negative root-function with a low slope (fig.14 Q=7.5 [m^3/s] design & Q=8.0 [m^3/s] design). Like the free vortex design the whole behavior is mirrored around the design point distribution. The angular velocity is rising from hub to shroud (fig.14 Q=5.0 [m^3/s] design & Q=5.5 [m^3/s] design).

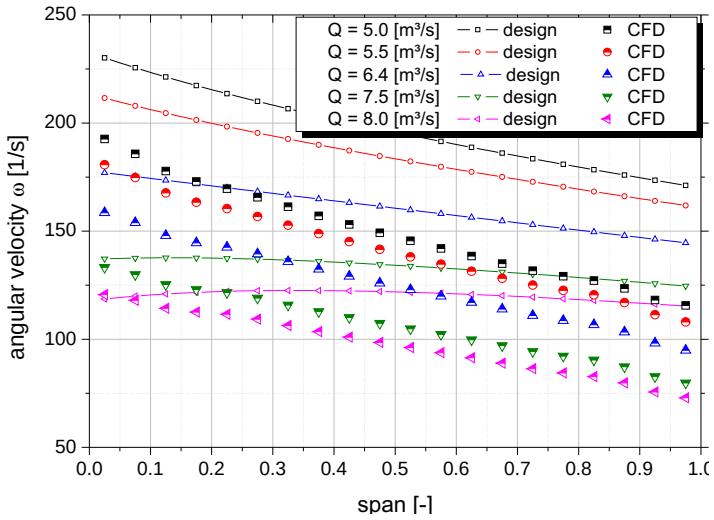

FIGURE 14. LINEAR ANGULAR VELOCITY ANGULAR VELOCITY DISTRIBUTION

All the angular velocity distributions of the CFD simulation possess qualitatively the same shape: High values at the hub, reducing toward the shroud (fig.14 Q=5.0 [m^3/s] CFD - Q=8.0 [m^3/s] CFD). The difference of the angular velocity between hub and shroud gets less pronounced for higher flow rates. The CFD simulation reach the design goal of linear angular velocity at a flow rate of Q=8.0 [m^3/s] CFD. The impeller is working in *partial load* at the flow rates Q=5.0 [m^3/s] CFD- Q=7.5 [m^3/s] CFD. Consequently this distributions have to be compared with the design prediction at *partial load* (Q=5.0 [m^3/s] design & Q=5.5 [m^3/s] design). Those distributions show also a good consistence with the ones of the design

prediction.

Figure 15 shows the change in the meridional velocity due to different flow rates. The meridional velocity distribution of the linear angular velocity design is similar to the meridional velocity distribution of the constant angular velocity design. At the design case the meridional velocity is an almost linear curve with a positive slope (fig.15 Q=6.4 [m^3/s] design). In overload the meridional velocity distribution is pushed to a higher level with the same slope and same shape (fig.15 Q=7.5 [m^3/s] design & 15 Q=8.0 [m^3/s] design). In partial load the meridional velocity distribution is pushed to a lower level with the same slope and the same shape (fig.15 Q=5.0 [m^3/s] design & 15 Q=5.5 [m^3/s] design).

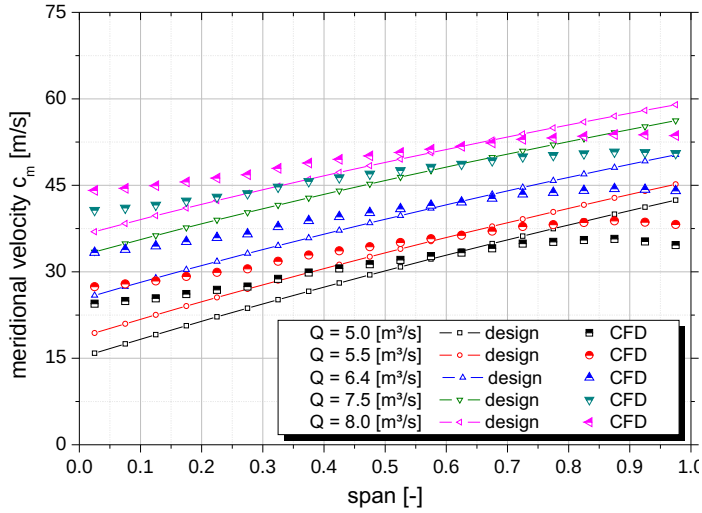

FIGURE 15. LINEAR ANGULAR VELOCITY MERIDIONAL VELOCITY DISTRIBUTION

The results of the CFD-simulation show also a linear meridional velocity distribution (fig.13 Q=5.0 [m^3/s] CFD - 15 Q=8.0 [m^3/s] CFD). But the slope of these distribution is lower compared to the slope of the design prediction. The angular velocity examination has shown, that the prescribed angular velocity distribution is achieved at a higher flow rate at a lower level. This difference results into a different slope for the meridional velocity (compare equation (14)). The prediction of a parallel shift of the meridional velocity distribution with the same slope of the design method is qualitatively fulfilled. In such a way a qualitatively consistence between the design prediction and the CFD-simulations for the forced vortex design of linear angular velocity is achieved.

Performance Characteristics

The total pressure characteristic is shown in figure 16. All three design methods have a linear total pressure increase with a negative slope. The free vortex design has the lowest total pressure increase of all three design models at the flow rate Q = 4.5 [m^3/s](f constant 16), but the highest increase at the flow rate Q = 8 [m^3/s]. The forced vortex designs have a steeper slope than the free vortex design with the constant angular velocity design having the steepest($\omega_f constant$ fig. 16). Both forced vortex designs differer only slightly in the total pressure characteristic.

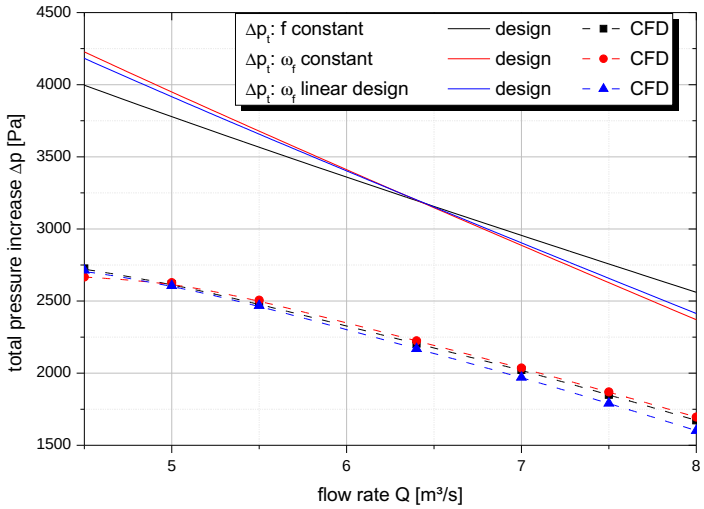

FIGURE 16. TOTAL PRESSURE CHARACTERISTIC

The CFD-simulation results do not reach the values of the design prediction. This is explainable due to the fact that none of this designs has reached the design requirement, considering the predictions for the angular velocity and angular momentum distributions. But the CFD-results show the trend of the total pressure increase characteristic qualitatively quite good. A slip factor is defined as follows:

$$\mu = \frac{\Delta p_{t,CFD}(Q)}{\Delta p_{t,1D}(Q)} \tag{42}$$

The plot of this slip factor is depicted in figure 17. The slip factor models the deviations between ideal and real flow behaviour with respect to the flow angles. All computed slip factors are not showing any discontinuities and the values do not scatter in a wide interval. The computed slip factor of the *free vortex design* shows values in the interval [0.65-0.69] f constant, the *(*forced vortex design) of constant angular velocity has values in [0.63-0.715] and the *(*forced vortex design) of linear angular velocity

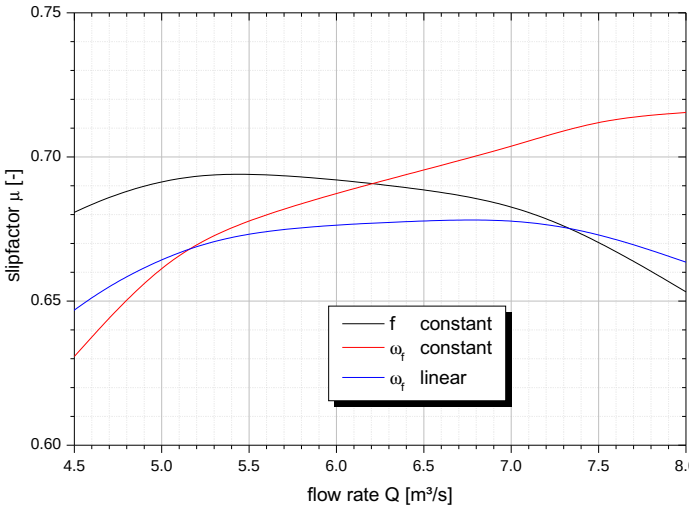

FIGURE 17. SLIP FACTOR

posses slip factor values at [64.8-65.2]. Calculating the slip factor according to the equations of Pfleiderer [11] results in the values depicted in table 3. These values were computed with the

μ	f	$\omega_{f,c}$	$\omega_{f,l}$
Pfleiderer	0.63	0.62	0.63
CFD	0.654 - 0.694	0.63 - 0.715	0.648 - 0.678

TABLE 3. SLIP FACTOR ACCORDING TO PFLEIDERER

help of this equation:

$$\mu = \frac{1}{1 + \frac{\chi \cdot \left(1 + \frac{\bar{\beta}_2(\bar{r})}{60^\circ}\right) \cdot \bar{r}}{z \cdot l}} \tag{43}$$

with

$$\bar{r} = \sqrt{\frac{r_a^2 + r_i^2}{2}} \tag{44}$$

χ is a free parameter, it has to be chosen out of the interval $[1, 1.2]$. For this calculation the value of 1 was used. Comparing this calculated prediction values with the ones obtained through this analysis it can be seen, that the new values are qualitatively in the same range. These results emphasize the validity of this new prediction method. An accurate calculation method for the slip factor and a comparison of this calculated slip factors with the prediction of Pfleiderer is prepared by the authors for publication (GT2011-46352, Smith at. al [12], Papers submitted for publication). One result of this analysis is, that the slip factor prediction based on empirical data from Pfleiderer is predicting the slip factor quite good. The total-to-static pressure increase characteristic is shown in figure 18. The comparison of design prediction and CFD results show a qualitatively good match. The shape of the depicted functions, CFD as well as design, is a negative parable for all three design methods.

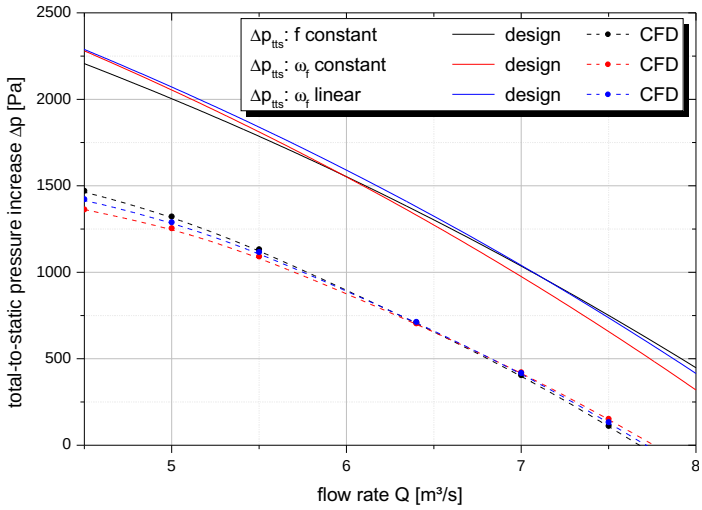

FIGURE 18. TOTAL-TO-STATIC PRESSURE CHARACTERISTIC

CONCLUSION AND OUTLOOK

The validation of the design prediction with CFD computations have shown that this prediction method provides a good qualitative estimation of the off-design behavior of the fan. The way in which the angular momentum distribution and the meridional velocity distribution is changing for different flow rates are consistent with the CFD results presented. The method is capable of predicting the total and total-to-static pressure characteristic. Furthermore, it is independent of the design model. For free vortex as well as for forced vortex models good results were obtained. Differences between design prediction and CFD-results occur due to the difference between ideal flow and real flow. The design prediction is working with the assumption of an infinite number of blades and a strictly blade congruent flow. Both conditions are not fulfilled by the real flow. Deviations between flow angle and blade angle can always be observed. Moreover the calculation is done with 17 blades, so differences between ideal one dimensional flow and CFD-simulation were expected. This prediction method enables the designer to investigate the

flow behavior at any flow rate. So the designer has a possibility to compare ideal flow calculations – obtained by this method – with the real flow CFD. It can be analyzed were the design condition is meet. Furthermore noticeable problems in the real flow can be detected and analyzed and corrected . The important fact here is that the analytical solutions will guide the designer safely in the right direction in order to get the best design. The advantage of this method is, that there are no loss models needed, which in general will work only for a certain class of impellers and a certain blade geometry. The designer can investigate the blade geometry, and its influence of the pressure characteristics. With the help of a quasi-3D methods like the ones that will be presented by two coauthors of this paper (currently prepared for publication GT2011-46352 [12] , GT2011-45860 [13]) a further improvement of the blade geometry could be obtained, and the difference between design prediction and CFD-simulation could be minimized.

NOMENCLATURE

MAIN CHARACTER

c	$[m/s]$	absolute velocity
w	$[m/s]$	relative velocity
u	$[m/s]$	rotational velocity
ω	$[1/s]$	angular velocity
f	$[m^2/s]$	angular momentum
Q	$[m^3/s]$	volumetric flow
ψ	$[-]$	local head coefficent
φ	$[-]$	local flow coefficent
p	[Pa]	pressure
ρ	$[k/m]^3$	density
m	$[-]$	hub to tip ratio
n	$[1/s]$	number of revolutions

SUBSCRIPTS

0	design Point
1	bladeinlet
2	bladeoutlet
t	total pressure
tts	total-to-static pressure
ti	tip
imp	impeller
f	fluid
k	constant angular momentum
c	constant angular velocity
l	linear angular velocity

REFERENCES

[1] Eck, B., 1972. *Ventilatoren*, 4^{th} ed. Springer-Verlag, Berlin, Germany.

[2] Eckert, B., and E.Schnell, 1980. *Axial- und Radialkompressoren*, 2^{th} ed. Springer-Verlag, Berlin, Germany.

[3] Lakshminarayana, B., 1996. *Fluid Dynamics and Heat Transfer of Turbomachinery*, 1^{st} ed. John Wiley & Sons, New York City, USA.

[4] Carolus, T., 2009. *Ventilatoren*, 2^{th} ed. Vieweg+Teubner, Wiesbaden, Germany.

[5] Lewis, R., 1996. *Turbomachinery Performance Analysis*, 1^{st} ed. Verlag John Wiley & Sons, New York City, USA.

[6] Boyce, W., and DiPrima, R., 2008. *Elementary Differential Equations*, 9^{th} ed. John Wiley & Sons, Denver, USA.

[7] Epple, P., Miclea, M., Luschmann, C., and Delgado, A., 2009. "An extended analytical and numerical desing method with applications of radial fans". In Proceedings of the ASME 2009 International Mechanical Engineering Congress & Exposition, ASME. IMECE2009-11283.

[8] Epple, P., Karic, B., Illic, C., Becker, S., Durst, F., and Delgado, A., 2008. "Design of radial impellers: a combined extended analytical and numerical method". *Journal of Engineering Manufacture Part C: J. Mechanical Engineering Science*.

[9] Epple, P., Durst, F., and Delgado, A., 2010. "A theoretical derivation of the cordier diagram for turbomachines". *Journal of Engineering Manufacture Part C: J. Mechanical Engineering Science*. reviewed and accepted, waiting for publishing.

[10] Menter, F., 1993. "Zonal two equation k-ω turbulence models for aerodynamic flows". *AIAA* 24^th *Fluid Dynamics Conference*(AIAA-93-2906).

[11] Pfleiderer, C., and Petermann, H., 1972. *Stroemungsmaschinen*, 7^{th} ed. Springer-Verlag, Berlin, Germany.

[12] Smith, H., Epple, P., Semel, M., Miclea, M., and Delgado, A., 2011. "Accurate calculation of the slip factor of axial cascades and impellers for arbitrary blade shapes". In Proceedings of the ASME 2011 International Mechanical Engineering Congress & Exposition, no. GT2011-46352,submitted and prepared for publication, ASME.

[13] Miclea, M., Smith, H., Epple, P., Semel, M., and Delgado, A., 2011. "Application of an inverse cascade analytical and numerical design method used in the design of axial fans". In Proceedings of the ASME 2011 International Mechanical Engineering Congress & Exposition, no. GT2011-45860,submitted and prepared for publication, ASME.